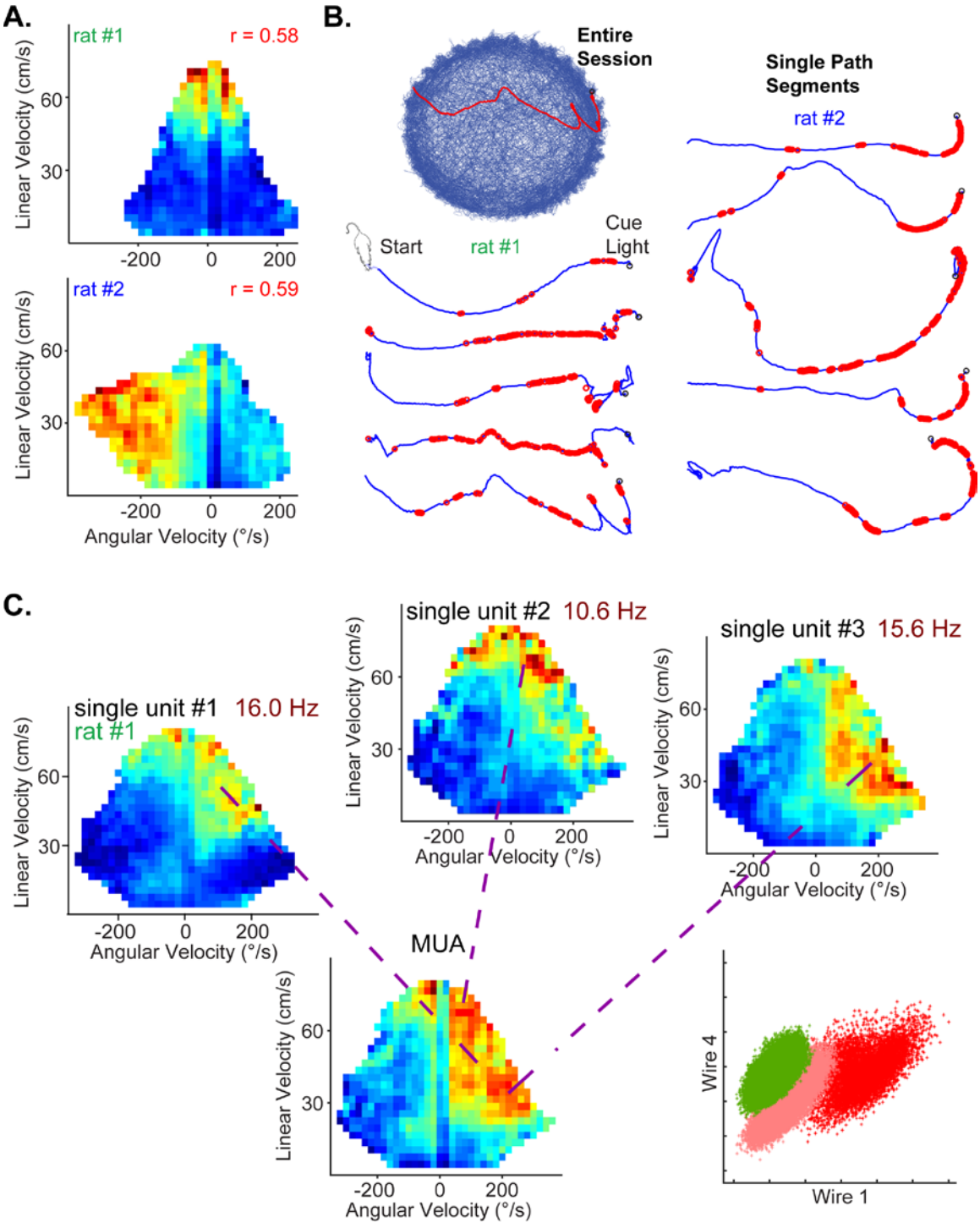

Figure S1. Spike path plots illustrate self-motion rate maps and self-motion tuned single units generally contribute to specific subsets of the slightly broader MUA tuning. Related to Figure 1. A. Example from rat #1 (*top*) of a multi-unit activity (MUA) data set tuned to linear motion of high velocity and from rat #2 (*bottom*) tuned to high left angular velocity. Within session correlation

values are listed in the top right corner of each self-motion plot in red. **B.** Tuning for a specific motion state is illustrated with five example trials where the rat made errors (i.e., did not run directly to the cue light). *Top Left*. Example of the entire session path plot (blue line) from which path segments are extracted (red line). Five examples of path segments for single trials for each rat/session were generated by placing a red circle on the path segment plot (blue line) for each spike that occurred when the activity rate was in the range for the motion tuning (*Left column:* linear velocity*; right column*: left angular velocity). Path segments were rotated for display purposes so the paths are parallel and so the start point is on the left and the end (the cue light) on the right. Path segments were selected from the random lights task for which it is easier to find trajectory deviations that illustrate the specificity of the tuning. **C.** Illustration of the observation that when multiple single cells are significantly tuned to self-motion on the same tetrode and the MUA on the same tetrode is also significantly motion tuned, single cells often represent different (single unit #2 vs #3) more narrow aspects of the slightly broader MUA tuning. Illustration is from rat #1. Single cell colormaps are evenly spaced standard colormaps ranging from zero (blue) to the peak firing rate (maroon), indicated in the top right corner for each putative single unit. *Inset, Lower Right.* Energy for a combination of 2 of the 4 tetrode wires is shown for each of the 3 example single units (red, pink and green). This projection summary (which was used in conjunction with a large array of additional information to “spike sort” these units) suggests that the effect shown is not likely to be a result of poor spike sorting. Note, MUA also includes several additional isolated units and spike data in addition to the subset of the single unit data shown here.

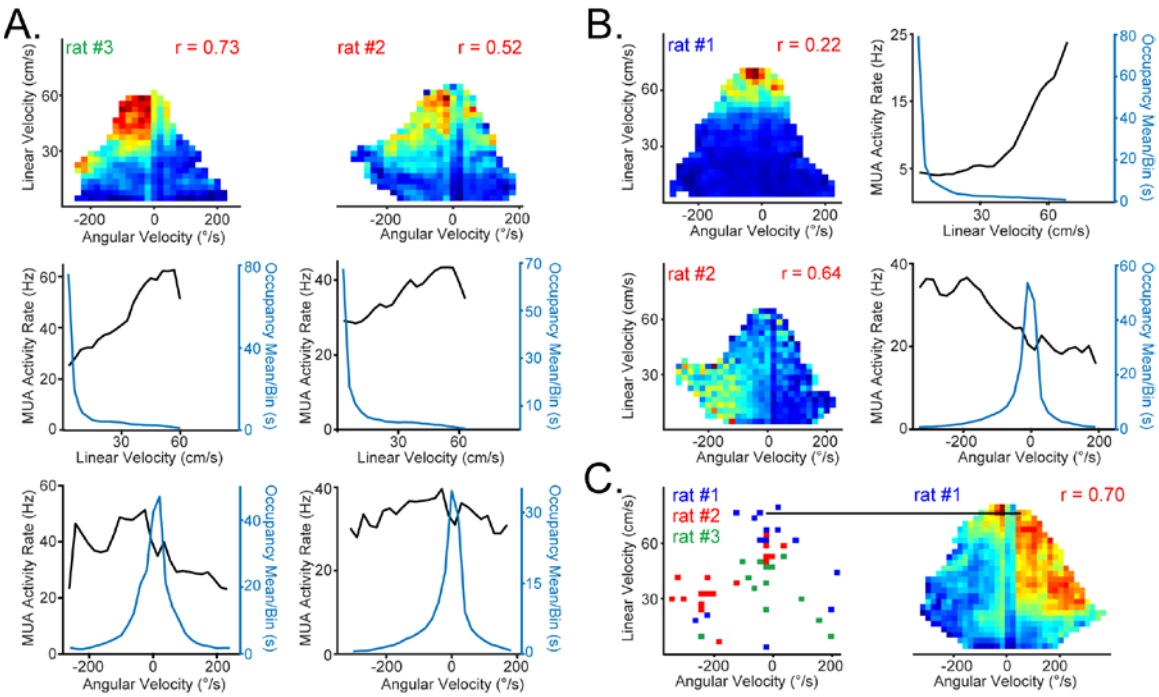

Figure S2. Motion tuning was not explained by occupancy. **Related to Figure 1.** Motion state tuning can occur for many different combination of high or low occupancy for linear and angular velocity. Extremely high occupancy produces a small dip in firing rate in some cases; however, there is no systematic correspondence between occupancy and peaks in firing rate. Firing rate profiles vary considerably across different tetrodes while occupancy profiles do not. In other words, occupancy does not appear to influence the apparent motion state tuning reported here. **A.** Two examples of MUA with a large variance in firing rate along both the linear and angular velocity axes. *Left.* Example from rat #3 with motion tuning that corresponds with low occupancy for angular velocity and linear velocity. *Right.* Example from rat #2 with medium occupancy for angular and low occupancy for linear velocity. **B**. Two examples of MUA with firing rates that vary mostly along one axis, either linear or angular velocity. For these examples, firing rate can correspond to low linear velocity occupancy (*top*) or low-left angular velocity (*bottom*). **C**. The peak bin from the rate map with the highest within session stability for each tetrode is shown for each rat as a proxy for the preferred tuning for that module. The data for all rats cover the full range of motion tuning, however, right turn tuning was not observed in rat #2, possibly as a result of a strong tendency to turn left at the reward zone, even when the goal location and their ultimate trajectory took them in a direction that would have been closer if the rat had simply turned to the right. Note the left asymmetry on most plots for this rat. It is possible the tetrodes in rat #2 that never met the criteria for motion modulated would be revealed to be right turn modules in the appropriate behavioral context. An example of a motion map with a line pointing to the corresponding data point is shown (*Right*).

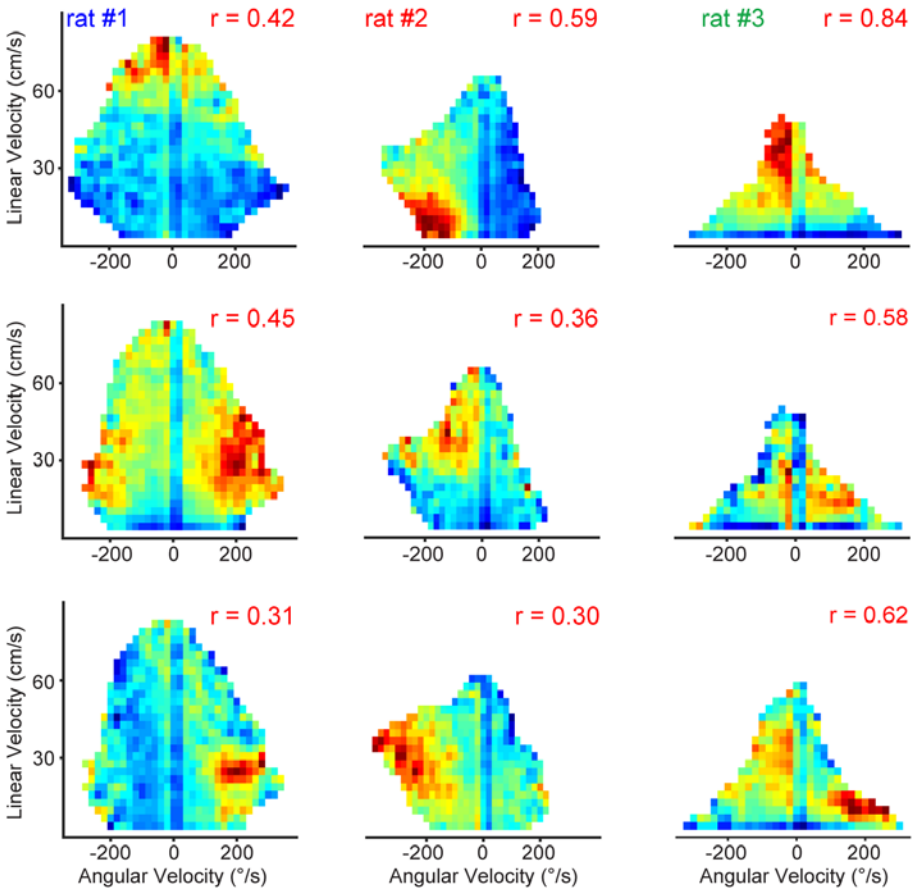

Figure S3. MUA motion map examples for each rat. Related to Figure 1. Multi-unit activity recorded for a single day's recording session and from a single tetrode were classified as having a preferred-self motion state if the self-motion maps for two behavioral sessions (from the whole day recording session) were significantly positively correlated. Occupancy data and number of spikes were binned according to linear velocity (vertical axis) and head angular velocity (horizontal axis; positive head angular velocity corresponds to a right turn), then converted to activity rate (number of multi-unit spikes per second) to produce each plot. The within session stability correlation value for each motion map is shown in the upper right corner of each motion activity rate map in red. The nine examples shown are of data from tetrodes from each of the 3 rats that were not shown elsewhere in the manuscript. Motion maps for three example tetrodes from each rat are shown for rat #1 (*Left Column*), rat #2 (*Middle Column*), and rat #3 (*Right Column*).

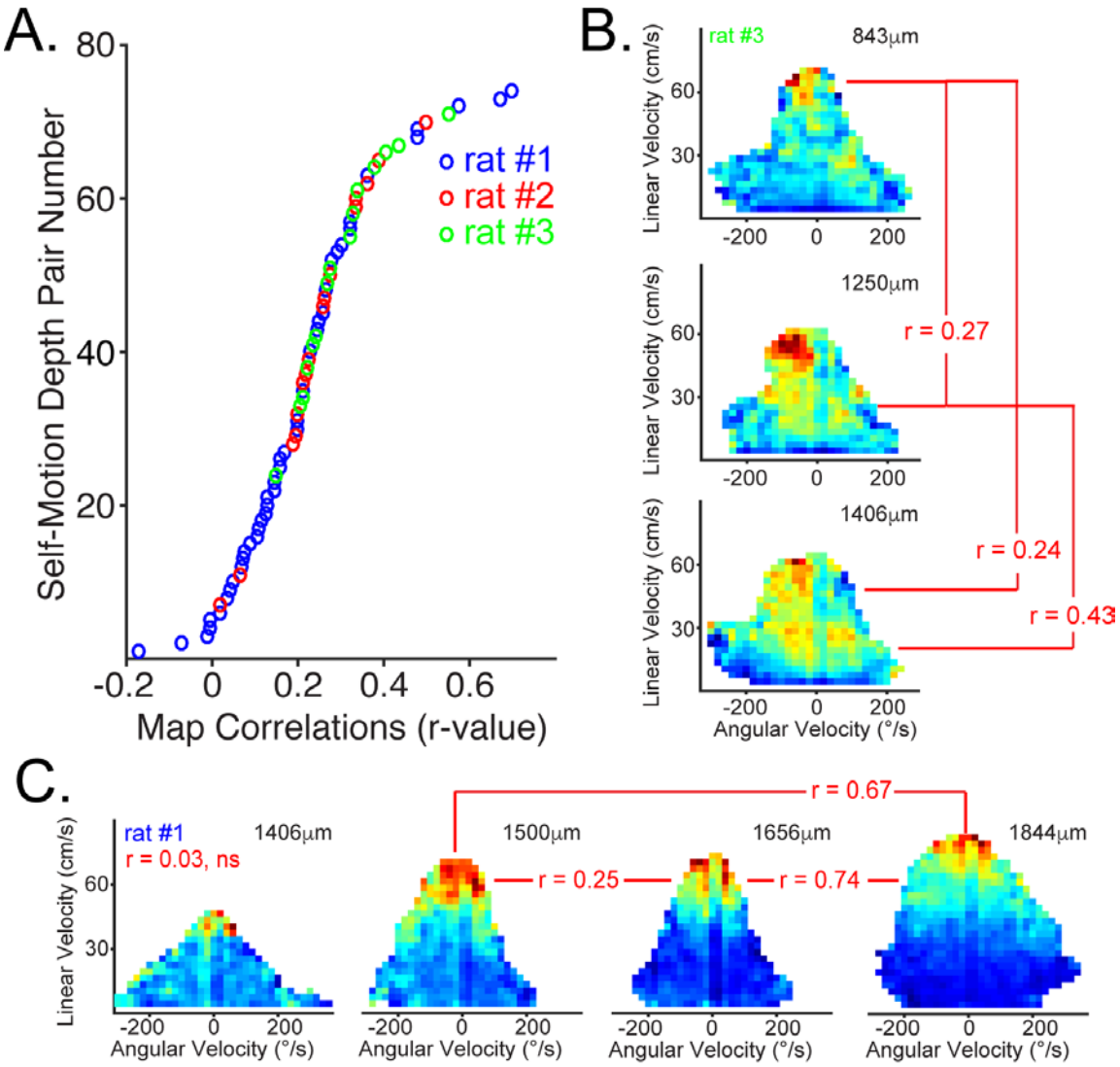

Figure S4. Depth correlation profile was similar and present across a large range of depths for each rat. **Related to Figure 1. A.** The sorted correlation value for each MUA cluster for each pair of depths where the tetrode was moved at least 100μm and the session data for each depth met the significance criteria as described in **Figure 1** are shown for each rat. Rat #2 had more depth correlations, but also had the most tetrodes in parietal cortex during the experiment. **B.** Same as in **Fig. 1C**, except **Fig. 1C** show data for rat #2, and data for rat #3 are shown here. Data came from two separate recording sessions obtained when the tetrode was at two different depths (843μm *above,* 1250μm *middle,* and 1406μm *below*). Note, even small correlations that only slightly exceeded the shuffled distribution critical value appear to correspond to MUA with visibly similar turning across depth. Only common data points were used for each pairwise comparison (e.g., see black outline on **Fig. 1C**). **C.** Same as in **B**, except data are for rat #1 and a fourth MUA data set is shown that did not meet the criteria for within session stability (*left*) and thus was not included in the depth correlation analysis. Note, despite the lack of significance this data is visibly

similar to the remaining three depth profiles that did meet the within session stability criteria. It appears that a lack of corresponding motion state data caused the lack of significance for the data set on the left, likely because this MUA came from the first day of training on the random lights task. As in **B**, even small depth correlations that only slightly exceeded the shuffled distribution critical value appear to correspond to MUA with visibly similar tuning across depth. The four examples shown here span 18 days of training. More days cannot be shown because the tetrode was turned into corpus callosum following the 1844μm MUA data set.

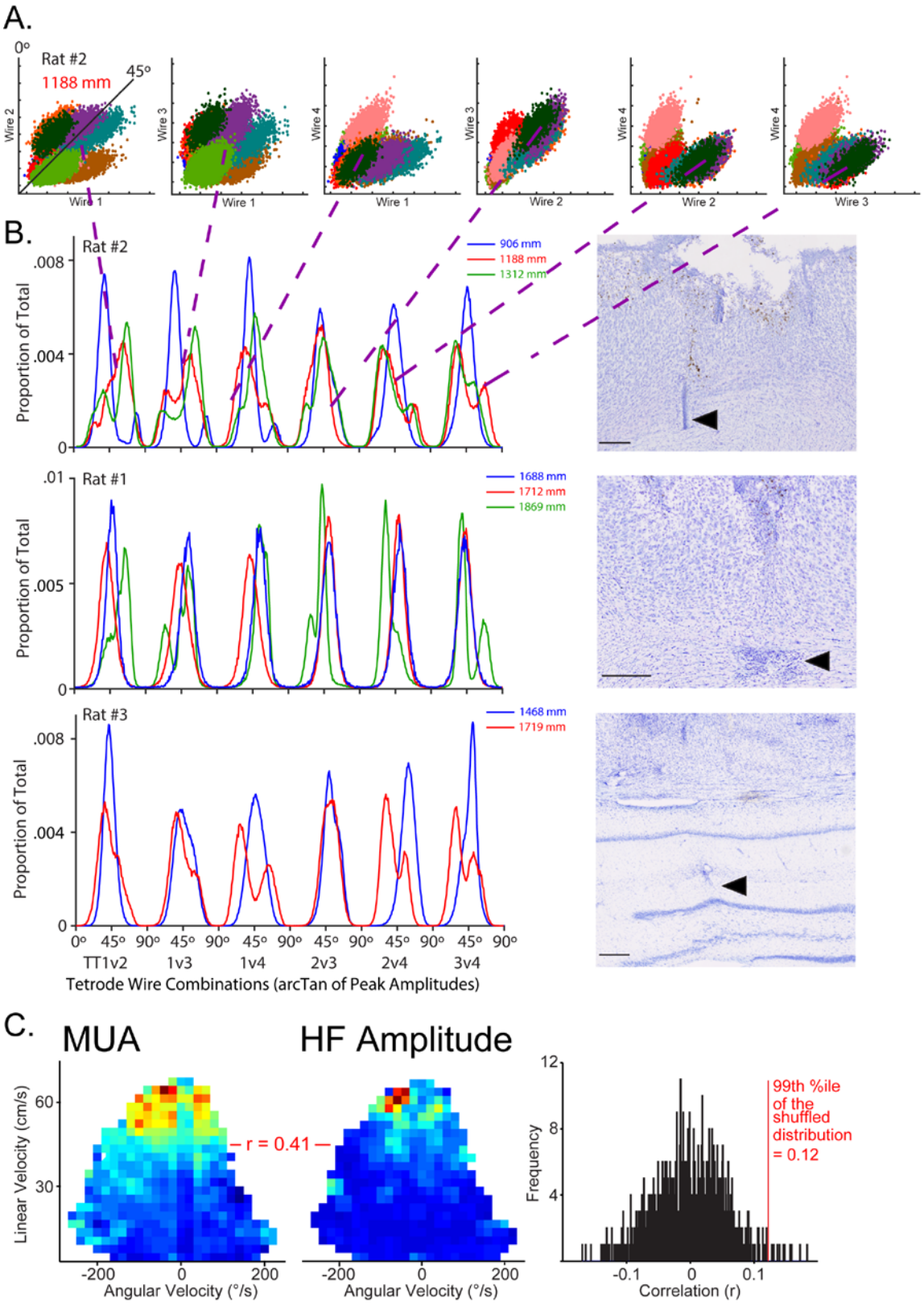

Figure S5. Tetrode amplitude spacing, histology, and observations of audio/visual signals during the experiment all suggest tetrodes used for

the data reported here were moving smoothly and accurately through the full depth of parietal cortex and illustration that high frequency (HF) amplitude and multiunit activity (MUA) maps can be highly correlated .
Related to Figure 1. A. Peak amplitude plots for each pairwise wire combination for the 1188μm depth recording session (red line in **B, *top***). Only data from well-isolated single units are shown. These data were spike sorted for previous analyses (Wilber et al., 2014) and thus blind to the present analyses. **B.** *Left.* The arctangent of each data point for each pair of tetrode wires was used to generate a histogram for all wire combinations for each recording session (normalized to total count). The value for each data point becomes the direction of that data point from 0º (horizontal) to 90º (vertical). Only the histograms for each data set with significant depth correlations for all pairwise combinations are shown. Visual inspection of all histograms confirmed that the spike amplitude profile for each recording depth was unique. For rat #2, the single unit spike amplitude profile was collected from the same data sets as the MUA reported here. For the example for rat #1, there were two recording depths that met our criteria; the first depth also had well-isolated single cell data (1688μm) and previously spike sorted data was only available for data sets above and below the second recording depth. For rat #3, the single unit data shown match the MUA for the first depth (1688μm), but for the second depth, the single unit data shown was collected at 1719μm and the MUA was collected from a subsequent session that was 60μm lower. Note, while the profile for different depths sometimes overlap for some wire combinations, the overall profile across all wire combinations differs for different depths. *Right***.** Most tetrodes were driven through all layers of cortex before recordings were terminated and this was confirmed with histological analysis. One example from each rat is shown of a marking lesion demonstrating that the tetrode had traveled through the full span of parietal cortex. *Top*. A sagittal section for rat #2 is shown for a tetrode that penetrated all layers of parietal cortex (black arrow). Coronal sections are shown for a rat #1 (*middle*) tetrode penetrating through all layers of parietal cortex (black arrow) and for a rat #3 (*bottom*) tetrode that was driven to dentate gyrus. In addition, we found no histological evidence of oblique penetration of any tetrodes (examples are shown here and on **Fig. 3**). Scale bars=250μm. **C**. *Left and Middle*. Same as in **Figure 1A**; however data came from the same session but from either the multiunit activity from a single tetrode (l*eft*, MUA) or from the high frequency (HF) signal recorded from a single wire of the same tetrode (*middle*, HF Amplitude). *Right*. The shuffled distribution and critical r-value corresponding to the 99th percentile. Shuffling was performed for the two self-motion maps (MUA and HF-LFP signal) as described for the two maps shown in **Figure 1A**.

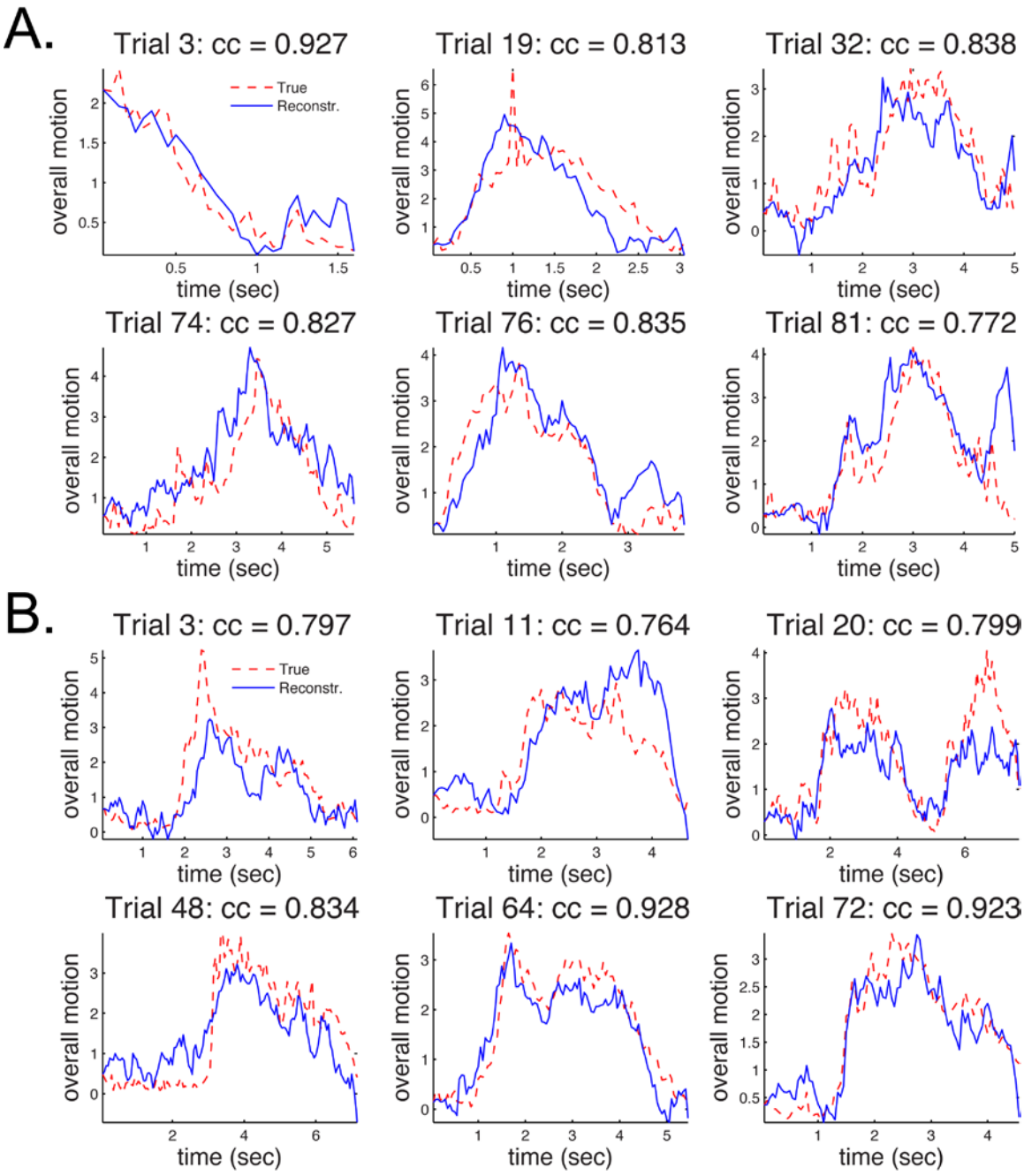

Figure S6. Neural decoding examples from 2 rats. **Related to Figure 1.** Data are shown for rat #1 (**A**) and rat #2 (**B**). Each plot shows true overall motion (a representation of the combination of linear and angular velocity, see methods) as a function of time (red dashed line) and reconstruction using the generalized linear model on multi-unit firing rates (blue solid line) in each example trial. The correlation coefficient (cc) between the true and reconstructed data are listed for each trial. For overall correlations, see **Table S1**.

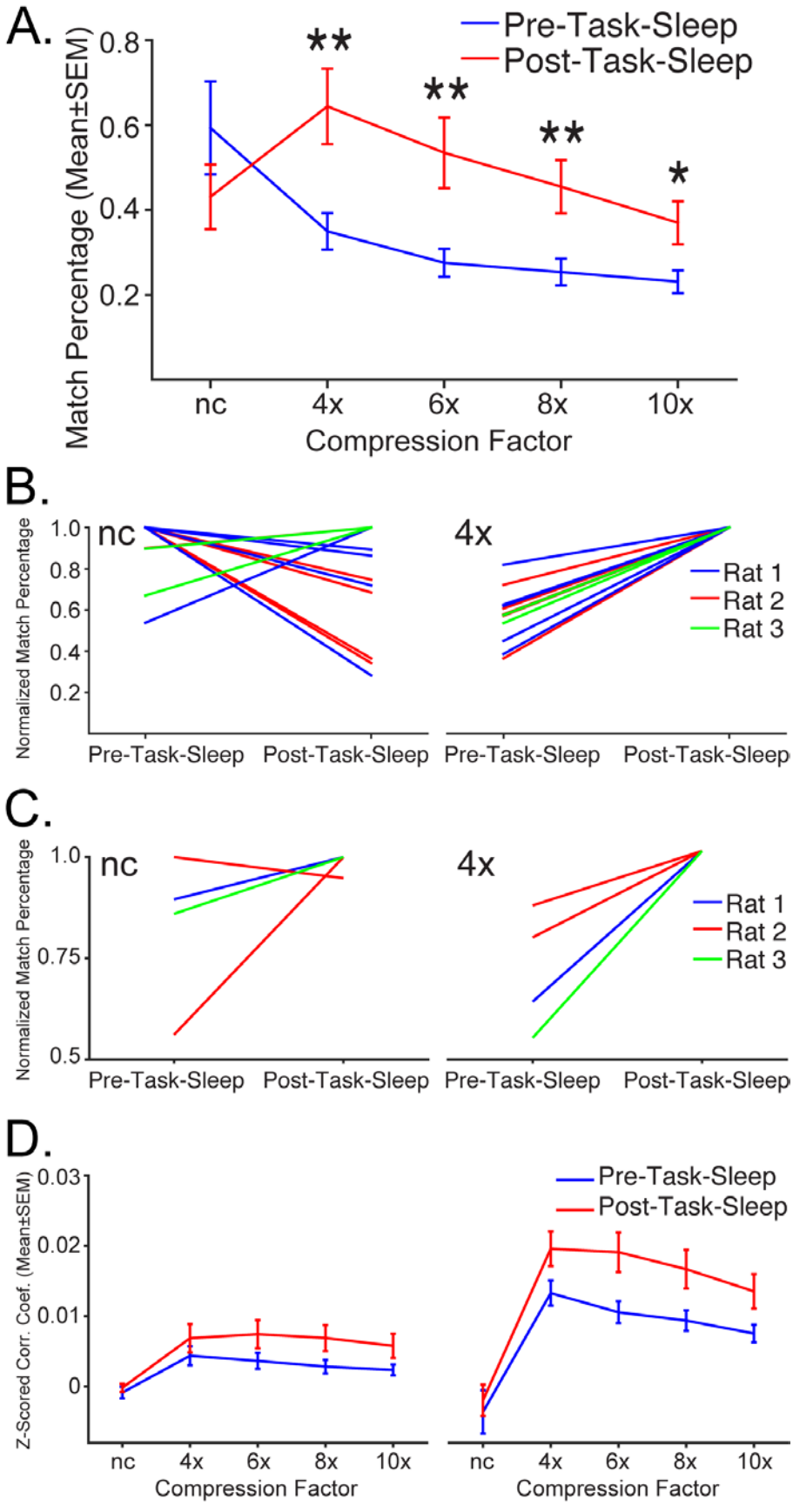
A.
Pre-Task-Sleep
Post-Task-Sleep
Match Percentage (Mean±SEM)
0.8
0.6
0.4
0.2
**
**
**
*
nc
4x
6x
8x
10x
Compression Factor
B.
Normalized Match Percentage
1.0
0.8
0.6
0.4
0.2
nc
4x
Rat 1
Rat 2
Rat 3
Pre-Task-Sleep
Post-Task-Sleep
Pre-Task-Sleep
Post-Task-Sleep
C.
Normalized Match Percentage
1.0
0.75
0.5
nc
4x
Rat 1
Rat 2
Rat 3
Pre-Task-Sleep
Post-Task-Sleep
Pre-Task-Sleep
Post-Task-Sleep
D.
Z-Scored Corr. Coef. (Mean±SEM)
0.03
0.02
0.01
0
Pre-Task-Sleep
Post-Task-Sleep
nc
4x
6x
8x
10x
Compression Factor
nc
4x
6x
8x
10x
Compression Factor

Figure S7. Modular sequence reactivation was observed using high frequency local field potentials (HF-LFP) and was enhanced around cortical delta waves and hippocampal sharp wave ripples. Related to Figures 4 & 5. **A.** Mean (±SEM) match percentage [(n matches/n time bins)*100] across compression factors for high frequency HF-LFP templates restricted to slow-wave sleep periods. Template matching increases between *pre*- (blue) and *post-task-sleep* (red) for compressed data, but not for 'no-compression' (nc). As with MUA, HF-LFP template reactivation measures peak at 4x compression and there was a significant interaction between sleep session and compression factor ($F_{(4, 44)}$=9.20, p< 0.001). **B**. Normalized match percentage (each value/peak session value) across nc, (*left*) and 4x (*right*) compression for HF-LFP templates during slow-wave-sleep for each session and rat. **C**. Same as **B**, but for single isolated cell template matching. For both the templates consisting of HF-LFP or single cell spike trains, match percentage consistently increases between *pre*- and *post-task-sleep* for compressed data, but not for nc. **D.** Mean (±SEM) event-triggered average Z-score for delta wave troughs (*left*) and sharp wave ripple peaks (*right*), for *pre-task-sleep* (blue) and *post-task-sleep* (red) with 4x compression. Both types of event-triggered template matching Z-score profile are similar to event-triggered profiles based on multiunit spiking activity (MUA)-based templates. Delta waves were preceded, while sharp wave ripples were followed by the prominent increases in matching Z-score. **E.** Mean (±SEM) event-triggered average Z-peak for delta wave (*left*) and sharp wave ripple (*right*) across the compression factors. *Right*. Sharp wave ripple-triggered average Z-peak amplitudes across the compression factors for HF-LFP templates. * p < 0.05, ** p < 0.01. *** p<0.001, **** p<0.0001.

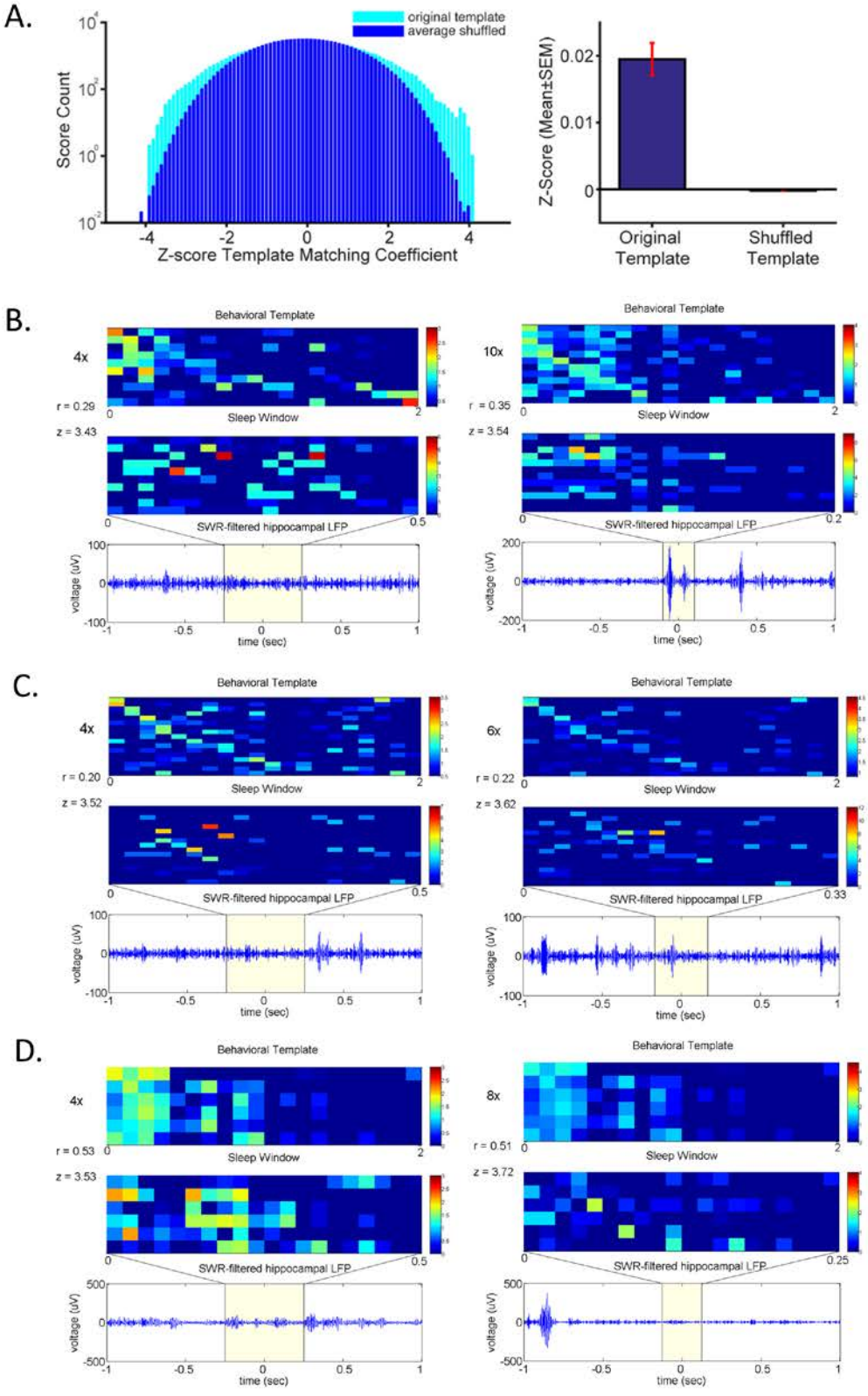
A.
original template
average shuffled
Score Count
Z-score Template Matching Coefficient
Z-Score (Mean±SEM)
Original Template
Shuffled Template
B.
Behavioral Template
4x
r = 0.29
z = 3.43
Sleep Window
SWR-filtered hippocampal LFP
voltage (uV)
time (sec)
10x
r = 0.35
z = 3.54
C.
4x
r = 0.20
z = 3.52
6x
r = 0.22
z = 3.62
D.
4x
r = 0.53
z = 3.53
8x
r = 0.51
z = 3.72

Fig. S8 Original versus shuffled template distribution and examples of sleep windows with high matching to behavioral template for each rat and across compression factors (4-10x). **Related to Figure 7. A.** *Left***.** Example histogram of Z-score distributions for the original template (blue) and average shuffled template (cyan). Distribution for the original template is broader, but slightly right skewed, reflecting the larger number of high values ('matches'). *Right***.** Mean (±SEM) Z-scores for the original and distribution of shuffled templates. Z-scores for the original templates are significantly higher ($p < 0.01$). n is number of datasets (n=12). **B-D.** *Top*: Behavioral template. Template consists of multineuronal spiking activity (MUA) or high frequency LFP (300-900 Hz) amplitude from multiple simultaneously recorded tetrodes during the last 2s of each trial, binned at 100ms and averaged over all the trials from a single behavioral session. Rows represent individual tetrodes and columns represent time bins. *Middle*: Sleep window with high matching to behavioral template. Sleep activity is processed in the same way as behavioral templates, except that the time bin size depends on the compression factor (range: 10ms for 10x compression to 100ms for 'no-compression'). *Bottom*. Hippocampal LFP, filtered in sharp wave/ripple (SWR) range (150-300 Hz), around the matching sleep window (yellow background). High matching events are temporally coupled with SWRs, but also ocurr without the temporal proximity to SWRs. r=Pearson correlation coefficient between the original behavioral template (top) and sleep window (middle). Z=Z-scored Pearson correlation coefficient. Z>3 is defined as significant match (reactivation event).

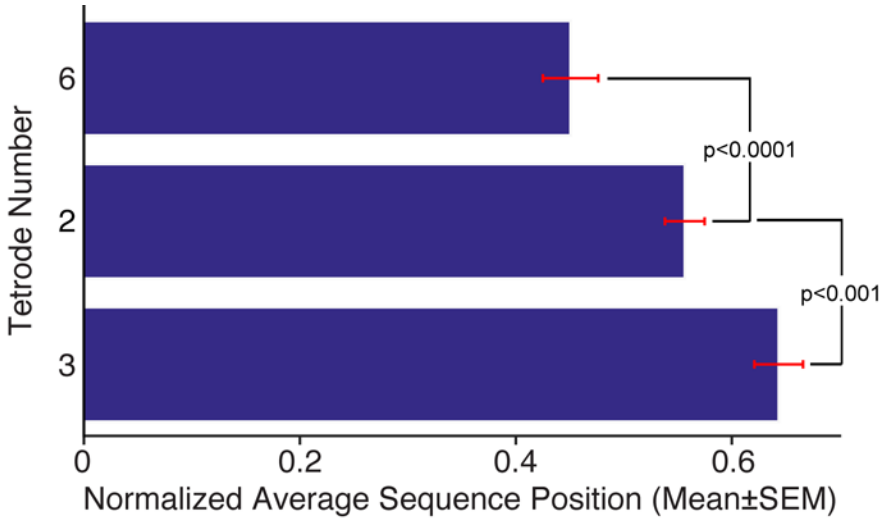

Figure S9. Example of sequential activity of the MUA from three simultaneously recorded tetrodes in parietal cortex. Related to Figure 2. Spike train center of mass latency ranks (Mean+/-SEM, normalized to sequence length; n of trials = 115). Latency ranks were obtained by first calculating the spike train center of mass latency, relative to window of interest (last 2s of each trial). Latencies were ranked on each trial, so the spike trains with shorter latencies were assigned lower rank (sequence position). Latency rank distributions were compared for each spike train pair. About 20% of spike train pairs had a significant difference in rank ($ps<0.005$, Bonferroni corrected for multiple comparisons), suggesting the temporal offset between the spike trains. In 58% of analyzed datasets, we found evidence for higher order sequences (triplets), where the first spike train (tetrode 6) latency rank was significantly smaller than the second spike train (tetrode 2), which was significantly smaller than the third spike train (tetrode 3).

Dataset	Decoding using MUA	Decoding using HF-LFP
Rat#1, Session 15	(0.58, 0.51)	(0.67, 0.62)
Rat#1, Session 18	(0.60, 0.61)	(0.72, 0.68)
Rat#2, Session 11	(0.60, 0.64)	(0.62, 0.64)
Rat# 2, Session 19	(0.63, 0.66)	(0.70, 0.69)

Table S1. Averaged decoding accuracy for combined data from all test trials. Related to Figure 1. The two numerical values in each entry (e.g., 0.58, 0.51) denote the averaged correlation coefficient over all testing trials for initial and cross-validated data, respectively. In each dataset, cross-validation was performed by alternatively using one behavioral session as training data and the other one as the test data. We note that the decoding performance is highly accurate in each dataset, and the HF-LFP-based model may slightly out-performs the spike-train-based model.

Rat Number	Mean	Standard Deviation (SD)	Median	Range	Number of MUA sets	Number of Data Sets
1	22	16	19	5-64	22	9
2	37	28	29	6-96	16	5
3	47	88	23	4-336	13	7
All Data (3 rats)	34	48	23	4-336	51	21

Table S2. Estimation of the number of cells per multi-unit activity (MUA) data set. **Related to Figures 1-3.** We made use of single unit data that was spike sorted for our previous paper (rats #1 and #2; Wilber et al., 2014) or spike sorted for unpublished analyses conducted several years earlier (rat #3). Data from each tetrode with significant MUA tuning stability that also had well-isolated single units (51 MUA data sets from 3 rats and 21 session data sets) were used to generate this table.

Rat Number	Mean	Standard Deviation (SD)	Median	Range	Number of MUA sets	Number of Data Sets
1	26	23	13	5-64	9	4
2	56	40	64	6-96	6	2
3	98	159	26	4-336	4	2
All Data (3 rats)	51	75	28	4-336	19	8

Table S3. Estimation of the number of cells per multi-unit activity (MUA) data set. **Related to Figures 4-5.** Same as **Table S2** except that only data from the 12 data sets that were used for memory reactivation analyses (19 MUA data sets from 3 rats and 8 session data sets) were used to generate this table.

	Pre-Task-Sleep	**Post-Task2-Sleep**
SWS duration (s)	1850 +/- 647	2484 +/- 349
REM duration (s)	141 +/-37	200 +/- 226
REM/SWS ratio	0.09 +/- 0.08	0.09 +/- 0.11

Table S4. Sleep architecture metrics for pre- versus post- task-sleep. Related to Figure 4. For the REM duration and REM/SWS ratio, there were not significant differences in pre- versus post- task-sleep ($ts_{(11)}<0.98$, $ps>0.35$). However, SWS duration was significantly greater in post-task-sleep (SWS duration: $t_{(11)}=2.23$, $p<0.05$).